CrossMark

J. Fluid Mech. (2018), *vol.* 848, *pp.* 968–986. © Cambridge University Press 2018
doi:10.1017/jfm.2018.369

An information-theoretic approach to study fluid–structure interactions

Peng Zhang[1], Maxwell Rosen[1], Sean D. Peterson[1,2] and Maurizio Porfiri[1,†]

[1]Department of Mechanical and Aerospace Engineering, New York University Tandon School of Engineering, Brooklyn, NY 11201, USA

[2]Department of Mechanical and Mechatronics Engineering, University of Waterloo, Waterloo, Ontario N2L 3G1, Canada

(Received 3 January 2018; revised 26 March 2018; accepted 28 April 2018; first published online 13 June 2018)

The question of causality is pervasive to fluid–structure interactions, where it finds its most alluring instance in the study of fish swimming in coordination. How and why fish align their bodies, synchronize their motion, and position in crystallized formations are yet to be fully understood. Here, we posit a model-free approach to infer causality in fluid–structure interactions through the information-theoretic notion of transfer entropy. Given two dynamical units, transfer entropy quantifies the reduction of uncertainty in predicting the future state of one of them due to additional knowledge about the past of the other. We demonstrate our approach on a system of two tandem airfoils in a uniform flow, where the pitch angle of one airfoil is actively controlled while the other is allowed to passively rotate. Through transfer entropy, we seek to unveil causal relationships between the airfoils from information transfer conducted by the fluid medium.

Key words: channel flow, flow–structure interactions, swimming/flying

1. Introduction

Nearly half of all fish species live a part of their life in a group (Pitcher 1998). This affords several advantages, including enhanced ability to escape from predators (Partridge 1982), searching for food (Pitcher, Magurran & Winfield 1982) and mating (Griffiths & Magurran 1998). Although it is difficult to disentangle the sensory cues underlying fish communication in groups, signals encoded in the flow have been proposed as determinants for the emergence of coordinated movements and stable formations (Weihs 1973).

Surprising results continue to challenge our intuition about the ‘hows’ and ‘whys’ of swimming in coordination. For example, while drafting results in drag reduction for the trailing body in a pair of rigid structures in a flow, so-called ‘inverted drafting’ has been observed for flexible structures (Ristroph & Zhang 2008), wherein the leader receives the hydrodynamic advantage at the expense of the follower. As another example, a dead animal trailing a bluff body can generate thrust

† Email address for correspondence: mporfiri@nyu.edu

https://doi.org/10.1017/jfm.2018.369 Published online by Cambridge University Press

through passive interaction with the wake of the bluff body (Liao 2007), thereby questioning the explanation of schooling based on lateral line sensing. Finally, it was recently discovered that the classical Weihs' diamond pattern (Weihs 1973) may be hydrodynamically inferior to a phalanx at high swimming speeds (Ashraf *et al.* 2017).

Beyond swimming fish, there is a need for principled approaches to infer cause-and-effect relationships from raw time series of multiple bodies oscillating in an encompassing fluid. Clusters of tall civil structures reacting to impacting vortices advected by the wind (Lam, Li & So 2003), arrays of active materials for underwater sensing and energy harvesting (Abdulsadda & Tan 2012; Hobeck & Inman 2012), nanomats of carbon nanotubes (Pozrikidis 2010), arrays of cilia for fluid mixing and transport (Ding *et al.* 2014) and antennulary setal hairs of copepods for mechanoreceptive sensing (Kiørboe *et al.* 2010) present fluid–structure interactions that are yet to be fully understood.

Here, we posit an information-theoretic approach to infer causality in fluid–structure interactions. The foundations of information theory date back to the seminal work of Shannon (1948), who introduced the concept of entropy to describe uncertainty of random variables. Grounded in information theory, nearly two decades ago, Schreiber put forward the concept of transfer entropy to isolate the driving and responding elements in coupled dynamical systems from their time series (Schreiber 2000). Briefly, transfer entropy measures the reduction of uncertainty in predicting the future state of a system (responding element) due to additional knowledge about the present state of the other system (driving element). In contrast to correlation-based approaches, inferences based on transfer entropy do not rely on a linear relationship between the coupled systems and are robust with respect to variations in interaction delays, making it suitable to unravel causality in fluid–structure interactions.

Since its inception, transfer entropy has found application in several domains (Bossomaier *et al.* 2016), from the identification of functional circuits in the brain (Vicente *et al.* 2011) to the analysis of financial markets (Marschinski & Kantz 2002), along with emerging studies on diffusion of policies in the United States (Anderson *et al.* 2016; Grabow *et al.* 2016; Porfiri & Ruiz-Marín 2018), cardiovascular and cerebrovascular regulation (Faes *et al.* 2013), climate networks (Hlinka *et al.* 2013) and collective behaviour of animals (Hu, Nie & Fu 2015; Orange & Abaid 2015; Butail, Mwaffo & Porfiri 2016; Tomaru *et al.* 2016; Nakayama *et al.* 2017).

For example, Orange & Abaid (2015) have demonstrated the possibility of reconstructing leader–follower interactions in pairs of bats flying in the wild from raw time series of the curvatures of their trajectories, reconstructed from three-dimensional (3D) tracking. Experimental results reported therein seem to support the intuition that bats occupying the frontal position in the pair tend to influence the behaviour of those in the rear position. Interestingly, a methodological comparison between transfer entropy and traditional cross-correlation to identify leaders in pairs of swimming fish has been presented in Butail *et al.* (2016), offering compelling evidence in favour of an information-theoretic approach to study causal relationships in animal behaviour.

Despite its promise, the possibility of employing transfer entropy to study causality in fluid–structure interactions has never been attempted. In contrast to the state of knowledge that relies on physical modelling of fluid flows and structural dynamics (Dowell & Hall 2001), transfer entropy may constitute a powerful, model-free approach to elucidate interactions from time series. The feasibility of an information-theoretic approach to the study of causal relationships

https://doi.org/10.1017/jfm.2018.369 Published online by Cambridge University Press

in fluid–structure interactions is grounded in prior work on geophysical fluid flows, where entropy-related notions have been proposed to assess the predictability of large-scale turbulence and quantify information content in ensemble predictions, from underlying physical models (Kleeman 2002, 2011; Majda, Kleeman & Cai 2002).

Toward demonstrating the validity of transfer entropy to detect causality in fluid–structure interactions in a model-free context, we focus on the archetype of tandem pitching airfoils. We consider two airfoils aligned in a uniform flow, wherein the pitch angle of one airfoil is actively controlled while the other passively rotates. The active control alternates the pitch angle based upon an underlying two-state ergodic Markov process, which generates an information-rich, aperiodic and stationary signal. We monitor the pitch angle of the airfoils to compute transfer entropy.

We formulate three hypotheses: (1) transfer entropy detects causality independent of which airfoil is actuated; (2) transfer entropy predicts that the influence decays with the distance between the airfoils; and (3) transfer entropy infers that the influence of the upstream airfoil on the downstream one is greater than the influence of the downstream airfoil on the upstream one. Hypothesis (1) evaluates whether the approach is robust in detecting causality with respect to the relative positioning of the airfoils, that is, directionality of the cause-and-effect relationship. Hypotheses (2) and (3) address the quantification of the degree of influence, that is, the relative magnitude of the cause-and-effect relationship, with respect to variations in the configuration.

This paper is organized as follows. A synoptic primer on transfer entropy is provided in § 2. Our experimental scheme and theoretical approach are introduced in § 3 and § 4, respectively. Results of transfer entropy analysis and assessment of its numerical stability are detailed in § 5. Conclusions from our major findings are presented in § 6.

2. Theoretical background

In information theory, the uncertainty of a discrete random variable, X, can be measured through the notion of entropy, originally defined by Shannon (1948) as

$$H(X) = -\sum_{x\in\Omega^X} \Pr\{X = x\} \log_2 \Pr\{X = x\}, \tag{2.1}$$

where $\Pr\{\cdot\}$ denotes probability, x is a realization of X, and the set Ω^X is the sample space that contains all possible realizations of X. The right-hand side of (2.1) corresponds to the expectation of the logarithm of the probability mass function, such that one may naturally define the joint and conditional entropies of two random variables, X and Y, as (Cover & Thomas 2006)

$$H(X, Y) = -\sum_{x\in\Omega^X, y\in\Omega^Y} \Pr\{X = x, Y = y\} \log_2 \Pr\{X = x, Y = y\}, \tag{2.2}$$

$$H(X \mid Y) = -\sum_{x\in\Omega^X, y\in\Omega^Y} \Pr\{X = x, Y = y\} \log_2 \Pr\{X = x \mid Y = y\}, \tag{2.3}$$

where y is a realization of Y and Ω^Y is the sample space of Y.

https://doi.org/10.1017/jfm.2018.369 Published online by Cambridge University Press

Given two stationary discrete stochastic processes, $X = \{X_t\}_{t\in\mathbb{Z}^+}$ and $Y = \{Y_t\}_{t\in\mathbb{Z}^+}$, in its basic incarnation, transfer entropy from X to Y is computed as (Schreiber 2000)

$$\begin{aligned}\mathrm{TE}_{X\to Y} &= H(Y_t \mid Y_{t-1}) - H(Y_t \mid Y_{t-1}, X_{t-1}) \\ &= \sum_{y_t, y_{t-1}, x_{t-1}} \Pr\{Y_t = y_t,\, Y_{t-1} = y_{t-1},\, X_{t-1} = x_{t-1}\} \\ &\quad \times \log_2 \frac{\Pr\{Y_t = y_t \mid Y_{t-1} = y_{t-1},\, X_{t-1} = x_{t-1}\}}{\Pr\{Y_t = y_t \mid Y_{t-1} = y_{t-1}\}},\end{aligned} \tag{2.4}$$

where $y_t, y_{t-1} \in \Omega^Y$ and $x_{t-1} \in \Omega^X$. Transfer entropy in (2.4) quantifies the reduction in the uncertainty of the prediction of the future state of Y from its present, taking into account additional knowledge about the present of X. In alignment with Wiener's principle of causality (Wiener 1956), such a reduction might be attributed to a cause-and-effect relationship between X and Y. If X has no influence on Y, the present of X does not encode information to predict Y; as such, transfer entropy should be zero. In contrast, if X influences Y, a non-zero transfer entropy should be detected, implying that predicting the future of Y is improved given knowledge of the present of X.

A generalization of (2.4) to account for delayed interactions between the stochastic processes has been recently established by Wibral *et al.* (2013). Given a delay $\delta \in \mathbb{Z}^+$, transfer entropy from X to Y is defined as

$$\begin{aligned}\mathrm{TE}_{X\to Y}(\delta) &= \sum_{y_t, y_{t-1}, x_{t-\delta}} \Pr\{Y_t = y_t,\, Y_{t-1} = y_{t-1},\, X_{t-\delta} = x_{t-\delta}\} \\ &\quad \times \log_2 \frac{\Pr\{Y_t = y_t \mid Y_{t-1} = y_{t-1},\, X_{t-\delta} = x_{t-\delta}\}}{\Pr\{Y_t = y_t \mid Y_{t-1} = y_{t-1}\}}.\end{aligned} \tag{2.5}$$

In this sense, transfer entropy quantifies the improvement in predicting the future of Y from its present, due to additional knowledge about X, δ time steps in the past. In our work, we focus on this definition to account for the finite speed of information transfer afforded by the encompassing fluid medium.

Through the information-theoretic construct of transfer entropy, we can infer cause-and-effect relationships in a principled manner that does not require an underlying mathematical model and inherently accommodates time-varying delays, stochasticity in measurements and nonlinear coupling. One of the key challenges for the application of transfer entropy on experimental data lies in the accurate estimation of the probability mass function from raw time series of finite length. The brute-force solution to estimate the probability mass function is to bin the datasets and count the occurrences of given triplets $(y_t, y_{t-1}, x_{t-\delta})$ in the two time series (Zhang & Grabchak 2013). This approach is simple to implement but it restrains the sample space based on the length of the time series, such that enough realizations of the stochastic processes are needed for estimating each bin of the distribution. The naive solution of increasing the acquisition frequency of the experiment to increase the length of time series might be pursued, but excessively fast acquisitions could magnify the effect of measurement noise (Paluš & Vejmelka 2007), thereby reducing the predicting power of transfer entropy.

To mitigate potential confounds associated with binning the time series and to deal with time series of moderate length, one may take on a symbolic approach to the computation of transfer entropy (Staniek & Lehnertz 2008). Symbolic representations are utilized in economics, medical science and genetics (Conaway 1989; López *et al.*

https://doi.org/10.1017/jfm.2018.369 Published online by Cambridge University Press

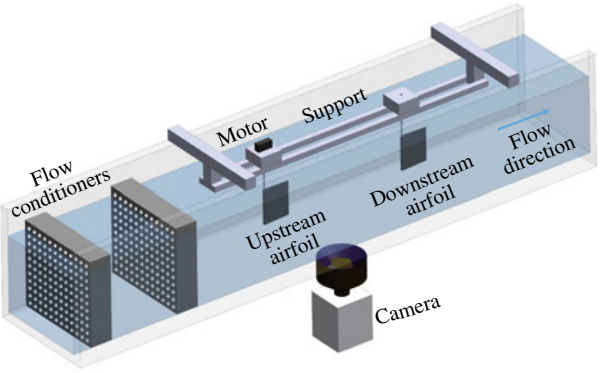


FIGURE 1. (Colour online) Schematic of the experimental set-up.

2010; Ruiz-Marín *et al.* 2010), where the relative change of the data rather than their precise magnitudes is important. In a symbolic approach to the computation of transfer entropy, we aggregate m consecutive steps of a time series into an m-history, $\{x_i\}_{i=t}^{t+m-1}$. Then, we order the m elements in increasing order and determine the permutation of the distinct indices $t_1, t_2, \ldots, t_m$ ranging from 0 to $m-1$, such that $x_{t+t_1} \leqslant x_{t+t_2} \leqslant \cdots \leqslant x_{t+t_m}$, and $t_s < t_{s+1}$ $(s = 1, 2, \ldots, m-1)$ if $x_{t+t_s} = x_{t+t_{s+1}}$. The tuple $(t_1, t_2, \ldots, t_m)$ is called a symbol and there are at most $m!$ symbols that can be generated from m-histories. For example, in a binary representation of the time series $\{x_t\}_{t=1}^{N}$ of length N, we could associate the symbol 1 if $x_t \leqslant x_{t+1}$ and -1 when $x_t > x_{t+1}$. Therefore, computing transfer entropy for binary symbols reduces to the estimation of only $2^3 = 8$ values for the probability of all the possible triplets. Further technical details on the implementation of symbolic transfer entropy can be found in Porfiri & Ruiz-Marín (2017) for the study of animal behaviour.

3. Experiments

Two identical 3D-printed NACA 0012 airfoils with chord lengths $c = 5$ cm and spans of 7 cm are situated in tandem in the centre of an open-channel water flume (Engineering Laboratory Design, Inc.) with test section 15 cm $\times$ 15 cm $\times$ 240 cm (see figure 1). Each airfoil weighs 10.9 g and has an effective density of 0.80 g cm^{-3}. As a result of the finite resolution of 3D printing, the trailing edges of the airfoils have a thickness of 0.7 mm. The flow is conditioned by two honeycomb flow straighteners prior to entering the test section. The free stream is set to $V = 3.0$ cm s^{-1}, which is verified using a Dantec Dynamics laser Doppler velocimetry system. At room temperature, this corresponds to a Reynolds number of $Re = Vc/\nu = 1500$, where ν is the kinematic viscosity.

Each airfoil pivots about its 12 % chord location via an aluminium rod that passes out of the tunnel and into an aluminium block with two press-fit stainless-steel ball bearings. A stainless-steel retainer ring maintains the vertical positioning. The blocks are adjusted to accommodate separation distances between the airfoils (L). Each airfoil can be either actively controlled by a servo-motor (Futaba S3004), or passively rotate with low friction. In active control, the motor is triggered by an Arduino Uno through the Arduino support package in MATLAB R2017a. With a time step Δt_{act}, a random binary number is generated with equal probabilities, which determines the pitch angle of the airfoil ($-15°$ or $15°$ with respect to the free stream) during the following

https://doi.org/10.1017/jfm.2018.369 Published online by Cambridge University Press

time step. The pitch angle of each airfoil is recorded over 300 s by a Nikon D7000 camera at 30 frames per second, at a resolution of 1280×720 pixels, with a maximum field of view of 37 cm $\times$ 21 cm. To facilitate tracking, fiducial marks (green tape) are placed at 5 % and 50 % chord of each airfoil.

As a preliminary step towards the systematic analysis of fluid-induced coupling of the airfoils, we verify the accuracy of transfer entropy predictions on synthetic interactions. Specifically, we consider two control conditions, in which both the airfoils are actively controlled. In both conditions, we set $L/c = 0.5$ and $\Delta t_{act} = 0.5$ s. In the first control condition ('Independently Active'), the actuation of the airfoils is independent of each other, and in the other one, the downstream airfoil is actuated in response to the upstream one with a prescribed time lag ('Coordinately Active'). For Coordinately Active, the actuation of the downstream airfoil follows the upstream airfoil with a time lag ΔT with probability $(1 - p)$, and with probability p it takes the opposite angle. We consider three different lags $\Delta T = 0.67$, 1.28 and 1.90 s, with $p = 0.1$, 0.19 and 0.29, respectively, such that the probabilities scale linearly with the time lags and weaker interactions are associated with longer time lags. Ten repetitions are conducted for Independently Active and for each time lag in Coordinately Active, totalling 40 trials. Through transfer entropy analysis, we expect to demonstrate that the airfoils do not influence each other in Independently Active. For Coordinately Active, we expect to identify that: the upstream airfoil influences the downstream airfoil, the degree of influence decreases with increasing delay, and the synthetic lag aligns with the time delay at which transfer entropy predicts the strongest interaction.

To demonstrate the application of transfer entropy in the study of fluid-induced coupling, we release the constraint that both the airfoils are actively controlled. Five separation distances, $L/c = \{0.2, 0.5, 1, 2, 5\}$, and two experimental conditions are studied. In the first condition, the upstream airfoil is active and the downstream airfoil is passive ('Upstream Active'), and, in the second, the roles of the airfoils are reversed ('Downstream Active'). For Upstream and Downstream Active, we consider three values of the time step in between actuation events, $\Delta t_{act} = \{0.5, 1, 2\}$ s. Ten repetitions are executed for each actuation condition, separation distance and time between actuation events, totalling 300 trials.

In control and experimental conditions, the time series of the pitch angles are extracted from the videos by a custom image analysis program. In each frame, the fiducial marks on the airfoils are identified from the green component of the image. The centroid of the two marks is then used to determine the pitch angles of the airfoils, which are collected for approximately five minutes, that corresponds to $N \approx 9000$ time instants given the frame rate of 30 frames per second. We use t to label the frame, and the physical time at t is $T(t)$, which we non-dimensionalize by a characteristic convective time scale $T_0 = c/V = 1.67$ s. Alternatively, one may non-dimensionalize with respect to the separation distance. This choice would be consistent with a convection-based explanation of the interaction, which would be tenable for condition Upstream Active but not for Downstream Active.

Before delving into the computation of transfer entropy and the results of our systematic analysis, it is of value to provide an overview of the underpinning fluid dynamics and concurrent foils' motion. An illustration of the flow fields in the Upstream and Downstream Active conditions measured using a Dantec Dynamics time-resolved planar particle image velocimetry (PIV) system is presented in figure 2. The flow is seeded with polyamide particles with a diameter of 50 μm and a density of 1.0 g cm^{-3}. The PIV system consists of a 100 mJ pulse^{-1} Nd:YAG dual-pulse laser with a wavelength of 532 nm, a Phantom high-speed camera and a timer box.

https://doi.org/10.1017/jfm.2018.369 Published online by Cambridge University Press

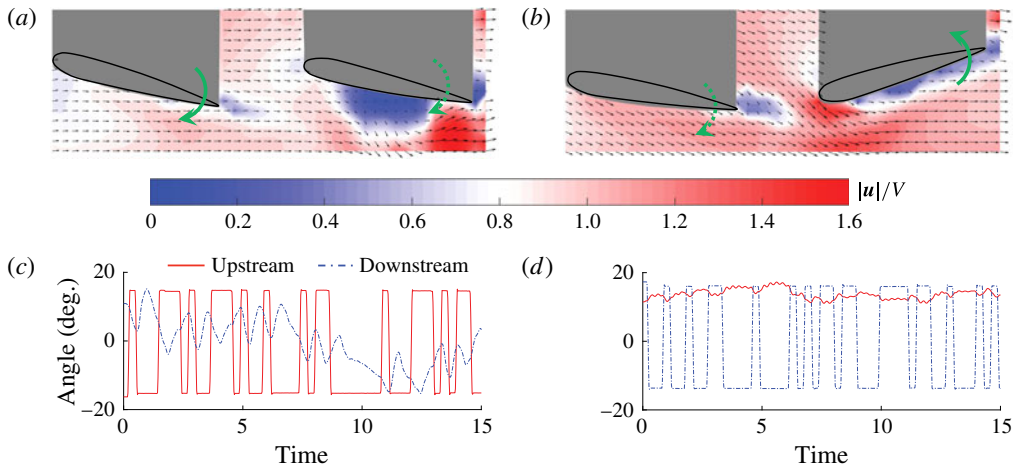


FIGURE 2. (Colour online) Fluid velocity field ($\boldsymbol{u}$) from the PIV measurements for (*a*) Upstream Active and (*b*) Downstream Active at $L/c = 0.5$ and $\Delta t_{act}/T_0 = 0.3$. In (*a*), the upstream airfoil has completed a clockwise flap, and the downstream airfoil is rotating clockwise. In (*b*), the downstream airfoil has completed an anticlockwise flap, and the upstream airfoil is rotating clockwise. Grey areas represent shadowed regions where data could not be collected. Solid (dashed) arrows indicate active (passive) rotation. Segments of the time series of the pitch angles of both airfoils are shown in (*c*) and (*d*), for Upstream Active and Downstream Active, respectively, at $L/c = 0.5$. In (*c*) and (*d*) time is non-dimensionalized by T_0.

In both conditions, there is a primary flow from left to right in the free-stream direction, which is perturbed by the oscillations of the airfoils. In Upstream Active, the signature of a vortex, previously shed from the upstream airfoil, is observed at the mid-chord location of the downstream airfoil, causing a clockwise rotation. The time series of the pitch angles hint at a complex relationship between the oscillations of the two airfoils, which is unlikely to be identified by a correlation analysis due to the varying delays and nonlinear coupling between the time series. In Downstream Active, it is tenable that the motion of the downstream airfoil interacts with the wake of the upstream airfoil, causing a change in the pitch angle (Strykowski & Sreenivasan 1990; Ozono 1999). Compared to Upstream Active, the interaction evidenced from the time series seems weaker. Through transfer entropy, we seek to unveil the complex relationship between the airfoils, shedding light on the direction, extent and time scale of the interaction.

4. Analysis

To mitigate the effect of measurement noise associated with the uncertainty in tracking the airfoils from the images and undesired mechanical vibration on the computation of transfer entropy, we downsample the time series of the pitch data with a resolution of f. Given the frame rate of 30 frames per second, two adjacent data points in the downsampled time series correspond to two frames that are $f/30$ seconds apart. Then, we convert m consecutive airfoil pitch angles to a symbol. For example, for $m = 2$, we encode each pair of consecutive pitch angles in a binary symbol, which is equal to 1 when the pitch angle increases and -1 when the pitch angle decreases.

https://doi.org/10.1017/jfm.2018.369 Published online by Cambridge University Press

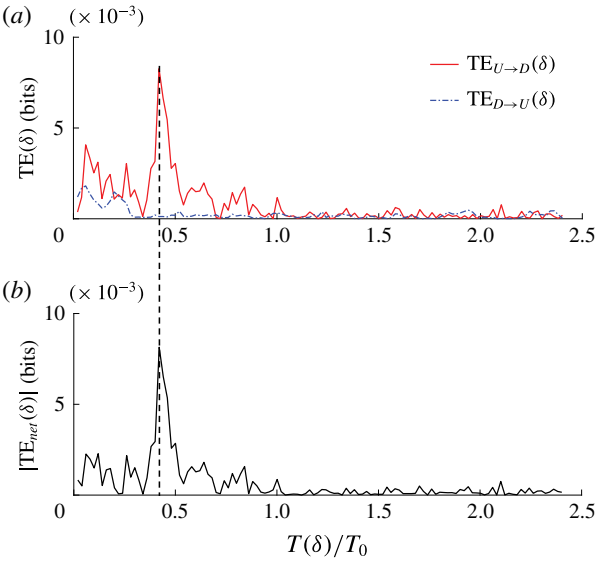


FIGURE 3. (Colour online) Plots of (*a*) $\mathrm{TE}_{U\to D}(\delta)$ and $\mathrm{TE}_{D\to U}(\delta)$ and (*b*) $|\mathrm{TE}_{net}(\delta)|$ as functions of $T(\delta)/T_0$. Values refer to the trial in Upstream Active illustrated in figure 2(*c*) for $m=2$ and $f=10$. The black dashed vertical line indicates the interaction delay δ_c.

The time series of symbols are denoted $\{u_t\}_{t=1}^{\lfloor N/f\rfloor}$ and $\{d_t\}_{t=1}^{\lfloor N/f\rfloor}$, for the upstream and downstream airfoils, respectively. On these sequences, we apply (2.5) to compute transfer entropy between the airfoils. Given the length of the time series, we limit our analysis to symbolic data generated with $m=2$ or $m=3$ consecutive frames and we systematically vary the resolution from 1 to 15.

Following Wibral *et al.* (2013), we expect that information flow between the two airfoils will be maximized in correspondence with the physical delay of their interaction. For each trial, we compute the delay that maximizes the magnitude of the net information transfer between the airfoils (see figure 3). Specifically, we evaluate $\mathrm{TE}_{net}(\delta)=\mathrm{TE}_{U\to D}(\delta)-\mathrm{TE}_{D\to U}(\delta)$ for time delay up to $T(\delta)/T_0=2.4$, search for the value of δ_c that maximizes $|\mathrm{TE}_{net}(\delta)|$, and extract $\mathrm{TE}_{U\to D}(\delta_c)$ and $\mathrm{TE}_{D\to U}(\delta_c)$. We refer to these two values as $\mathrm{TE}_{U\to D}$ and $\mathrm{TE}_{D\to U}$, whose relative magnitudes are indicative of the cause-and-effect relationship.

5. Results and discussion

This section summarizes the key findings of our experimental campaign. First, we present results on the control trials and then we turn to experimental conditions. To ease the discussion of experimental findings, we initially focus on a time step between actuation events $\Delta t_{act}=0.5$ s. Based on pilot testing, the treatment of both control and experimental data is based on binary symbols with a resolution $f=10$, resulting in approximately 900 symbols per time series. Upon gaining insight into the application of transfer entropy to study the physics of the problem, we move to a thorough robustness analysis, in which we systematically examine the influence of the resolution, number of symbols and time between actuation events.

https://doi.org/10.1017/jfm.2018.369 Published online by Cambridge University Press

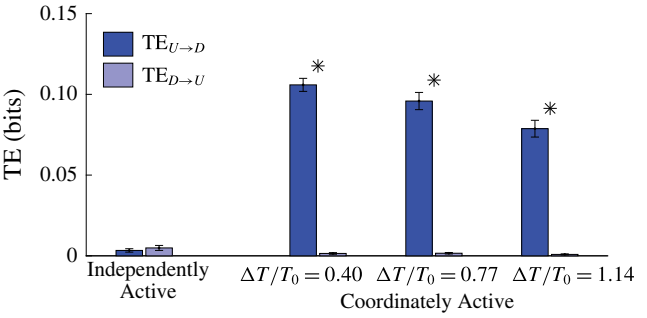


FIGURE 4. (Colour online) Transfer entropies $TE_{U\to D}$ and $TE_{D\to U}$ for control conditions, in which both the airfoils are simultaneously actuated. Computations are performed with $m = 2$ and $f = 10$. Error bars represent standard errors, and an asterisk identifies significant difference between $TE_{U\to D}$ and $TE_{D\to U}$ from paired t-tests (adjusted $p < 0.05$).

5.1. *Control conditions*

Figure 4 presents the values of $TE_{U\to D}$ and $TE_{D\to U}$ for control conditions. Predictably, for Independently Active, no significant difference between $TE_{U\to D}$ and $TE_{D\to U}$ is observed ($p = 0.49$ in paired t-tests). On the other hand, when the downstream airfoil motion is controlled by the upstream airfoil in Coordinately Active, we find that $TE_{U\to D} > TE_{D\to U}$ for all ΔT (adjusted $p < 0.01$ with Bonferroni correction (Abdi 2007) in paired t-tests). (Throughout the statistical analysis, we adjust all the p-values by Bonferroni correction to correct for multiple comparisons, thereby limiting the possibility of false positives, that is, claiming the presence of a significant finding in spite of its absence.) As a result, transfer entropy is accurate in identifying the existence and direction of cause-and-effect relationships that underlie the synthetic time series.

Not only is transfer entropy successful in determining that the upstream airfoil influences the downstream airfoil in Coordinately Active, but also it successfully infers that the degree of the influence decreases with increasing delay. In fact, linear regression indicates that $TE_{U\to D}$ is negatively dependent on $\Delta T/T_0$ ($TE_{U\to D} = -0.0367\Delta T/T_0 + 0.121$; $p < 0.01$ for t-statistics on slope). No dependence of $TE_{D\to U}$ on $\Delta T/T_0$ is revealed due to the modest values of the recorded entropy, with $p = 0.33$ for t-statistics on slope.

Finally, figure 5 confirms that transfer entropy accurately anticipates the lag of the interaction in Coordinately Active, whereby the predicted interaction time delay $T(\delta_c)$ closely follows the prescribed time lag ΔT.

5.2. *Experimental conditions*

Figure 6 illustrates aggregated data from the two experimental conditions. In agreement with our first hypothesis, we find that transfer entropy is successful in detecting the causal relationship underlying the observed pitching dynamics for both the conditions in which one airfoil is actuated. Specifically, we find that $TE_{U\to D} > TE_{D\to U}$ for Upstream Active (adjusted $p < 0.01$ in paired t-tests for all separation distances except for $L/c = 5$, when $p > 0.99$) and $TE_{U\to D} < TE_{D\to U}$ for Downstream Active (adjusted $p < 0.05$ in paired t-tests for $L/c = 0.2$ and $L/c = 0.5$; $p = 0.055$ for $L/c = 1$; $p = 0.057$ for $L/c = 2$; and $p = 0.66$ for $L/c = 5$). At $L/c = 5$, the minute values of transfer entropy hinder a statistical comparison, suggesting a

https://doi.org/10.1017/jfm.2018.369 Published online by Cambridge University Press

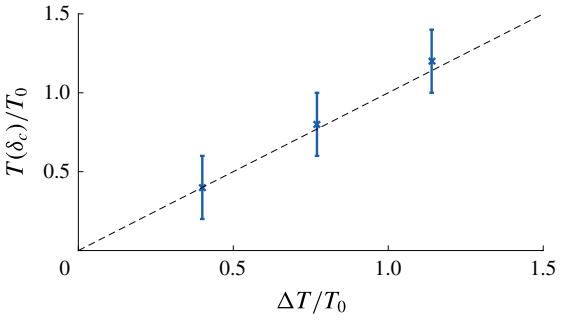


FIGURE 5. (Colour online) Non-dimensional interaction time delays predicted by transfer entropy in Coordinately Active. Computations are performed with $m = 2$ and $f = 10$. The dashed straight line is the bisectrix and error bars represent standard errors.

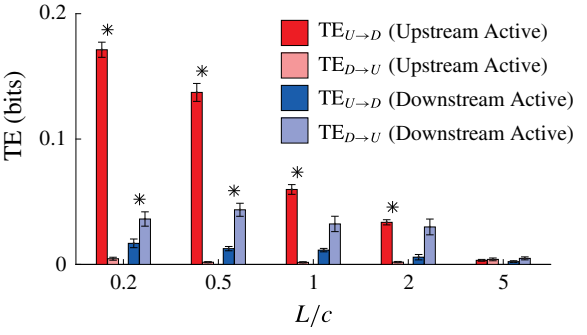


FIGURE 6. (Colour online) Transfer entropies $TE_{U\to D}$ and $TE_{D\to U}$ for the five separation distances and the two experimental conditions. Error bars represent standard errors, and an asterisk identifies significant difference between $TE_{U\to D}$ and $TE_{D\to U}$ from paired t-tests (adjusted $p < 0.05$). Data refer to a time step between actuation events $\Delta t_{act} = 0.5$ s, and computations are performed with $m = 2$ and $f = 10$.

modest interaction between the airfoils that explains the large p-value. Should both the airfoils be free to rotate, without actuation, the values of transfer entropies would be remarkably reduced, hampering the detection of a causal relationship between their motions – see additional experiments in the supplementary material.

To test our second hypothesis on the decay of the influence as a function of the separation distance, we study the dependence of the information transfer on L/c in both actuation conditions. We fit a linear regression on the values of the dominant transfer entropy ($TE_{U\to D}$ for Upstream Active and $TE_{D\to U}$ for Downstream Active) as a function of L/c. The analysis confirms that transfer entropy is negatively dependent on L/c (Upstream Active: $TE_{U\to D} = -0.0303L/c + 0.134$, $p < 0.01$ for t-statistics on slope; and Downstream Active: $TE_{D\to U} = -0.00728L/c + 0.0420$, $p < 0.01$ for t-statistics on slope).

To test our third hypothesis that the fluid flow favours information transfer in the downstream direction, we compare $TE_{U\to D}$ in Upstream Active and $TE_{D\to U}$ in Downstream Active for all values of L/c. Two-sample t-tests are performed at each L/c between the two conditions. We find that $TE_{U\to D}$ in Upstream Active is higher than $TE_{D\to U}$ in Downstream Active at $L/c = 0.2$, 0.5 and 1 (adjusted $p < 0.01$ in

https://doi.org/10.1017/jfm.2018.369 Published online by Cambridge University Press

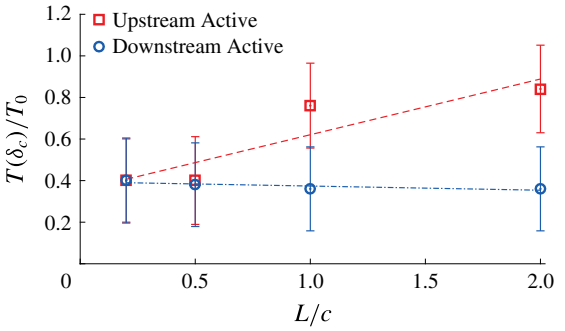


FIGURE 7. (Colour online) Non-dimensional time delay at which the magnitude of the net transfer entropy is maximized as a function of the separation length for Upstream Active and Downstream Active, superimposed with linear regression fits. Error bars represent standard errors. Data refer to a time step between actuation events $\Delta t_{act} = 0.5$ s, and computations are performed with $m = 2$ and $f = 10$.

two-sample t-tests). No difference is detected between $\mathrm{TE}_{U\to D}$ in Upstream Active and $\mathrm{TE}_{D\to U}$ in Downstream Active at $L/c > 1$ (adjusted $p > 0.99$ at $L/c = 2$ and 5 in two-sample t-tests).

In the open channel employed in the experiments, three physical pathways are likely to contribute to the hydrodynamic interaction between the airfoils: vortex advection, surface waves and acoustics. Vortices generated by the upstream airfoil advect downstream at approximately the free-stream speed and impact the downstream airfoil, causing unsteady pressure loading after a time lapse of approximately $T_0 L/c$. In addition to the formation of a trailing-edge vortex upon airfoil actuation, surface waves are generated in the open channel, offering a bidirectional communication pathway between the airfoils. Surface waves should propagate at $V_s \approx 1$ m s^{-1} ($V_s = \sqrt{gh}$, where g is the gravitational acceleration and h is the channel depth (Lamb 1945)), which would lead to a fast interaction with a time scale of $0.03 T_0 L/c$. Acoustics could also contribute to the bidirectional interaction, at an even faster time scale, comparable with the speed of sound in water.

To delve into the relative role of these pathways, in figure 7, we examine the dependence of the delay δ_c as a function of L/c; we exclude $L/c = 5$ due to the modest information transfer that challenges the inference of δ_c. In Upstream Active, we find a marked dependence of the delay on the separation distance ($T(\delta_c)/T_0 = 0.268 L/c + 0.353$, $p < 0.01$ for t-statistic on the slope), suggesting that the hydrodynamic interaction is supported by a combination of vortex advection and surface waves. In Downstream Active, no dependence between δ_c and L/c is found, consistent with the premise that vortex advection is not a feasible pathway for this condition. In addition to hydrodynamic pathways, there is potential for structural coupling due to mechanical vibration of the experimental facility. To exclude this possibility, we performed an experiment in which there was no water in the channel and found no detectable oscillation in the passive airfoil – see the additional trial in the supplementary material available at https://doi.org/10.1017/jfm.2018.369.

5.3. *Robustness analysis*

Here, we attempt to demonstrate the robustness of transfer entropy predictions across a range of potential variations in the set-up for the computation and actuation

https://doi.org/10.1017/jfm.2018.369 Published online by Cambridge University Press

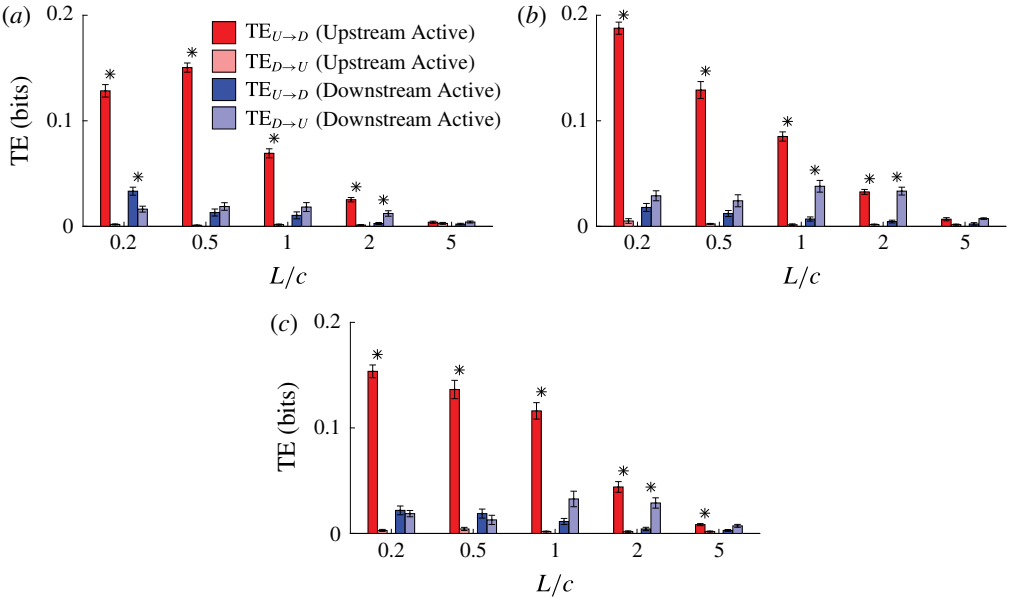


FIGURE 8. (Colour online) Effect of downsampling on $\mathrm{TE}_{U\to D}$ and $\mathrm{TE}_{D\to U}$ for the two experimental conditions with $\Delta t_{act} = 0.5$ s, at five separation distances using binary symbols ($m = 2$). Time series of pitch angles are downsampled at a resolution f of (*a*) 9, (*b*) 11 and (*c*) 12. Error bars represent standard errors, and an asterisk identifies significant difference between $\mathrm{TE}_{U\to D}$ and $\mathrm{TE}_{D\to U}$ from paired *t*-tests (adjusted $p < 0.05$). From comparisons, we find that $\mathrm{TE}_{U\to D} > \mathrm{TE}_{D\to U}$ for all but two Upstream Active combination and $\mathrm{TE}_{U\to D} < \mathrm{TE}_{D\to U}$ for most of the combinations considered in Downstream Active.

parameters. The statistical analysis precisely mirrors the framework proposed in § 5.2 with a consistent significance level of 0.05. For ease of presentation, details on the statistical analysis for this robustness study are included in the supplementary material.

First, we analyse the same dataset for $\Delta t_{act} = 0.5$ s considered earlier, but for varying choices of the resolution f. Again, we consider binary symbols in the computation of transfer entropy. Through a parametric analysis, we find that predictions on causality are consistent within the range $9 \leqslant f \leqslant 12$. In this range, transfer entropy computations lead to consistent predictions on the directionality, strength and time delay of the interaction between the two airfoils, thereby confirming the three hypotheses on which this study rests.

To support the claim on the consistency of directionality, we present values of $\mathrm{TE}_{U\to D}$ and $\mathrm{TE}_{D\to U}$ for both experimental conditions for $f = 9$, 11 and 12 in figure 8. With respect to the strength of the interaction, we find that $\mathrm{TE}_{U\to D}$ for Upstream Active and $\mathrm{TE}_{D\to U}$ for Downstream Active are negatively dependent on L/c (except for $\mathrm{TE}_{D\to U}$ for Downstream Active at $f = 12$). Comparison between $\mathrm{TE}_{U\to D}$ in Upstream Active and $\mathrm{TE}_{D\to U}$ in Downstream Active confirms that information transferred is favoured by the fluid flow, whereby $\mathrm{TE}_{U\to D}$ in Upstream Active is significantly higher than $\mathrm{TE}_{D\to U}$ in Downstream Active for $f = 9$, $L/c \leqslant 2$; $f = 11$, $L/c \leqslant 1$; and $f = 12$, $L/c \leqslant 1$. Finally, the dependence of the delay $T(\delta_c)$ on L/c for $f = 9$, 11 and 12 is examined through linear regression fits in figure 9. In Upstream Active, we confirm a marked dependence of the delay on the separation

https://doi.org/10.1017/jfm.2018.369 Published online by Cambridge University Press

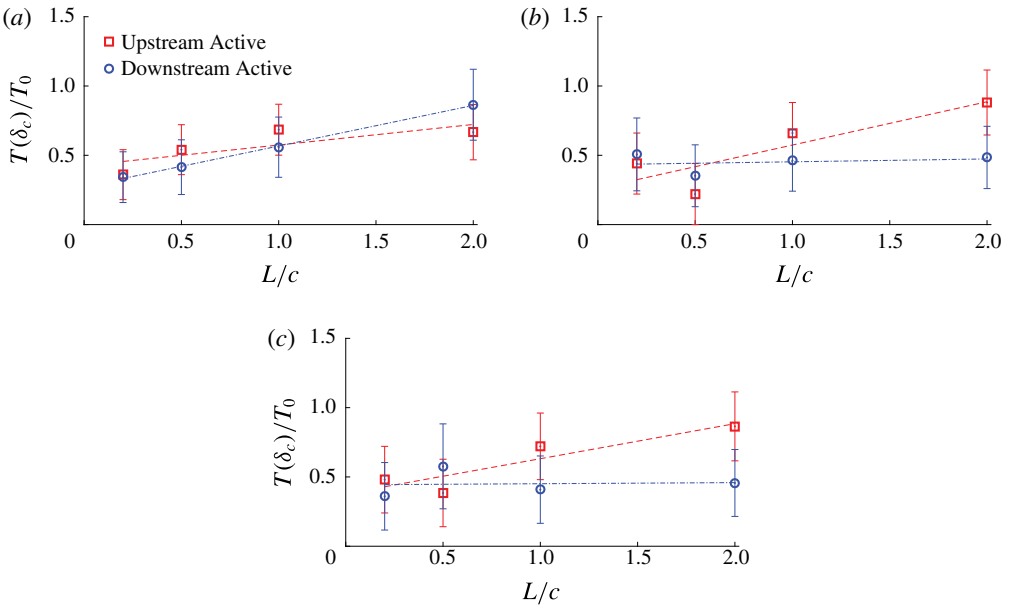


FIGURE 9. (Colour online) Effect of downsampling on non-dimensional interaction time delay predicted through transfer entropy for Upstream Active and Downstream Active with $\Delta t_{act} = 0.5$ s, using binary symbols ($m = 2$). Time series of pitch angles are downsampled at a resolution f of (*a*) 9, (*b*) 11 and (*c*) 12. The predicted values are superimposed with linear regression fits (red dashed line and blue dot-dashed line). Error bars represent standard errors.

distance for all the tested values of f, while in Downstream Active, no significant dependence of $T(\delta_c)$ on L/c can be established except for $f = 9$.

Next, we examine the effect of increasing the number of symbols in the representation of the time series, by studying the case $m = 3$. By comparing the relative value of three consecutive angles, we obtain six distinct symbols. For example, one symbol refers to the case in which the angle consistently decreases from the first to the third frame and another one indicates the case in which the first angle is higher than the other two, but the third is larger than the second one. Encoding the symbols in the time series for upstream and downstream pitch angles, respectively, we compute transfer entropy via (2.5).

Similar to the analysis for binary symbols, we systematically downsample the time series of pitch angles at resolutions up to $f = 15$ and find stable predictions within the range $5 \leqslant f \leqslant 8$. Overall, the parametric study demonstrates that, by using a symbolic representation of the time series of the pitch angle with six symbols rather than two, we attain equivalent conclusions, thereby offering further evidence for the reliability of our information-theoretic approach to study causality in fluid–structure interactions. The smaller resolutions ($5 \leqslant f \leqslant 8$) needed for treating the case $m = 3$ compared to $m = 2$ ($9 \leqslant f \leqslant 12$) could be attributed to two factors. First, increasing the number of symbols to six implies a drastic growth in the number of probabilities to be evaluated (216 for $m = 3$ versus 8 for $m = 2$), calling for more data points to be employed to accurately estimate transfer entropy. Second, considering three adjacent frames helps mitigating the effect of measurement noise, thereby affording the treatment of faster acquisitions.

https://doi.org/10.1017/jfm.2018.369 Published online by Cambridge University Press

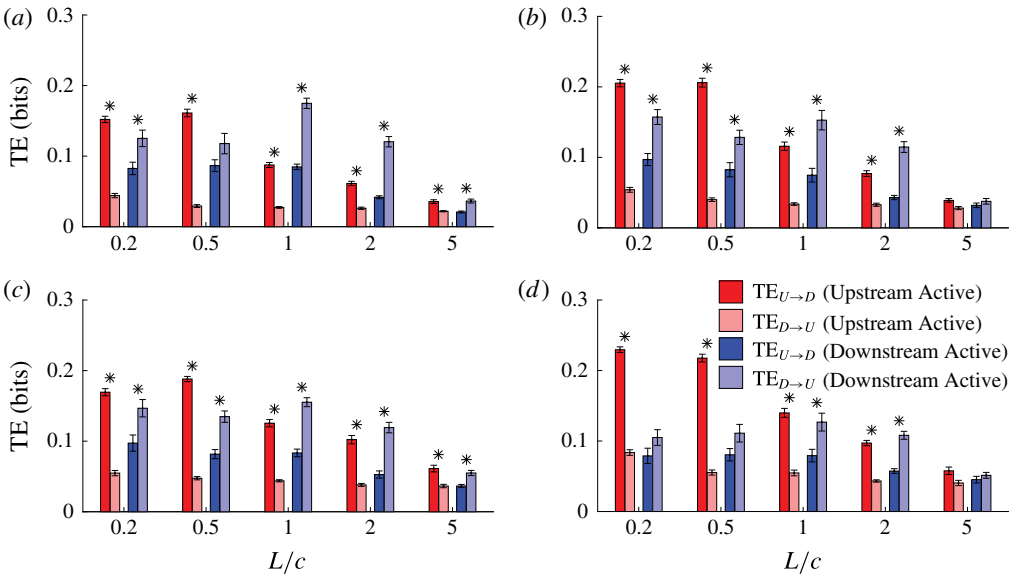


FIGURE 10. (Colour online) Effect of increasing the number of symbols to six ($m = 3$) on $\mathrm{TE}_{U\to D}$ and $\mathrm{TE}_{D\to U}$ for the two experimental conditions with $\Delta t_{act} = 0.5$ s, at five separation distances. Time series of pitch angles are downsampled at a resolution f of (*a*) 5, (*b*) 6, (*c*) 7 and (*d*) 8. Error bars represent standard errors, and an asterisk identifies significant difference between $\mathrm{TE}_{U\to D}$ and $\mathrm{TE}_{D\to U}$ from paired *t*-tests (adjusted $p < 0.05$). From comparisons, we find that $\mathrm{TE}_{U\to D} > \mathrm{TE}_{D\to U}$ for all but two Upstream Active combination and $\mathrm{TE}_{U\to D} < \mathrm{TE}_{D\to U}$ for most of the combinations considered in Downstream Active.

In favour of the consistency in the prediction of the directionality of the causal relationship, we present the values of $\mathrm{TE}_{U\to D}$ and $\mathrm{TE}_{D\to U}$ for both experimental conditions in figure 10. Supporting the robustness of predicting the strength of the interaction, we find that $\mathrm{TE}_{U\to D}$ in Upstream Active and $\mathrm{TE}_{D\to U}$ in Downstream Active conditions are negatively dependent on L/c. Comparison between $\mathrm{TE}_{U\to D}$ in Upstream Active and $\mathrm{TE}_{D\to U}$ in Downstream Active supports the propagation of information through the fluid flow, albeit to a lesser extent than the case of binary symbols. Specifically, we find that values of $\mathrm{TE}_{U\to D}$ in Upstream Active are significantly higher than $\mathrm{TE}_{D\to U}$ in Downstream Active for $f = 6$, $L/c \leqslant 0.5$; $f = 7$, $L/c = 0.5$; and $f = 8$, $L/c \leqslant 0.5$. The dependence of the delay $T(\delta_c)$ on L/c for $5 \leqslant f \leqslant 8$ is studied through linear regression fits in figure 11. For Upstream Active, we confirm a marked positive dependence of the delay on the separation distance for all f tested, and for condition Downstream Active, no significant dependence of $T(\delta_c)$ on L/c can be established for $f = 6$ and 7.

To demonstrate the robustness of transfer entropy predictions against variations of experimental parameters, we analyse independent trials with a larger time interval between actuation events, namely, $\Delta t_{act}/T_0 = 0.6$ and 1.2. We implement the analysis using binary symbols ($m = 2$) and resolution $f = 10$, based on the numerical set-up in §§ 5.1 and 5.2. The consistency of our predictions for different values of Δt_{act} offer compelling evidence in favour of our information-theoretic approach to study cause-and-effect relationships underlying fluid–structure interactions.

https://doi.org/10.1017/jfm.2018.369 Published online by Cambridge University Press

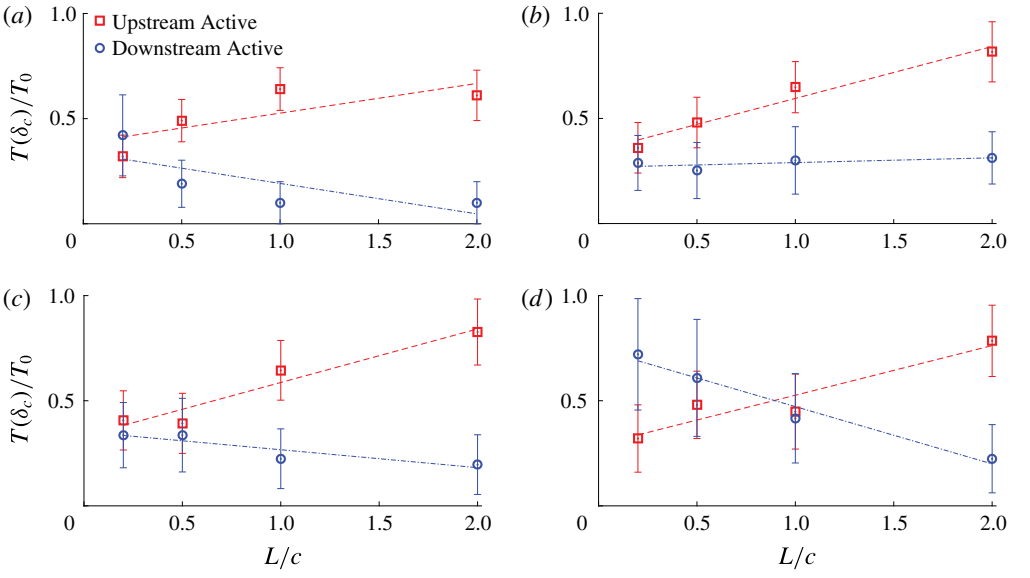


FIGURE 11. (Colour online) Effect of increasing the number of symbols to six ($m = 3$) on non-dimensional interaction time delay predicted through transfer entropy for Upstream Active and Downstream Active with $\Delta t_{act} = 0.5$ s. Time series of pitch angles are downsampled at a resolution f of (*a*) 5, (*b*) 6, (*c*) 7 and (*d*) 8. The predicted values are superimposed with linear regression fits (red dashed line and blue dot-dashed line). Error bars represent standard errors.

Results of the computation of transfer entropy and the interaction delay are synoptically presented in figure 12. Findings presented therein offer evidence in favour of the possibility to correctly determine causal relationships from experimental data with longer time intervals between actuation events. From the regression analysis, we find that $\mathrm{TE}_{U\to D}$ for Upstream Active and $\mathrm{TE}_{D\to U}$ for Downstream Active are negatively dependent on L/c, although we lose significance in the dependence of Downstream Active on $\Delta t_{act}/T_0 = 1.2$. The reason for the reduced statistical power at increased $\Delta t_{act}/T_0$ may be sought in the smaller number of meaningful events that are now available for inferring causality from the time series. For $\Delta t_{act}/T_0 = 1.2$, on average, each time series will contain 25 % of the actuation events of the time series for $\Delta t_{act}/T_0 = 0.3$. In favour of the possibility to evidence information transfer through fluid flow, we find that values of $\mathrm{TE}_{U\to D}$ in Upstream Active are significantly higher than $\mathrm{TE}_{D\to U}$ in Downstream Active for both $\Delta t_{act}/T_0 = 0.6$ and 1.2 (except for $\Delta t_{act}/T_0 = 0.6$, $L/c = 5$, and $\Delta t_{act}/T_0 = 1.2$, $L/c \geqslant 1$). Finally, from the study of the dependence of the delay $T(\delta_c)$ on L/c, we observe a marked positive correlation between the delay and the separation distance in Upstream Active, while a dependence of $T(\delta_c)$ on L/c cannot be established in Downstream Active.

6. Conclusion

In this study, we have posited a model-free approach to infer causality in a fluid–structure interaction problem from raw experimental data. Our approach is grounded in the information-theoretic concept of transfer entropy, which offers a powerful lens to explore information transfer in dynamical systems. Given two

https://doi.org/10.1017/jfm.2018.369 Published online by Cambridge University Press

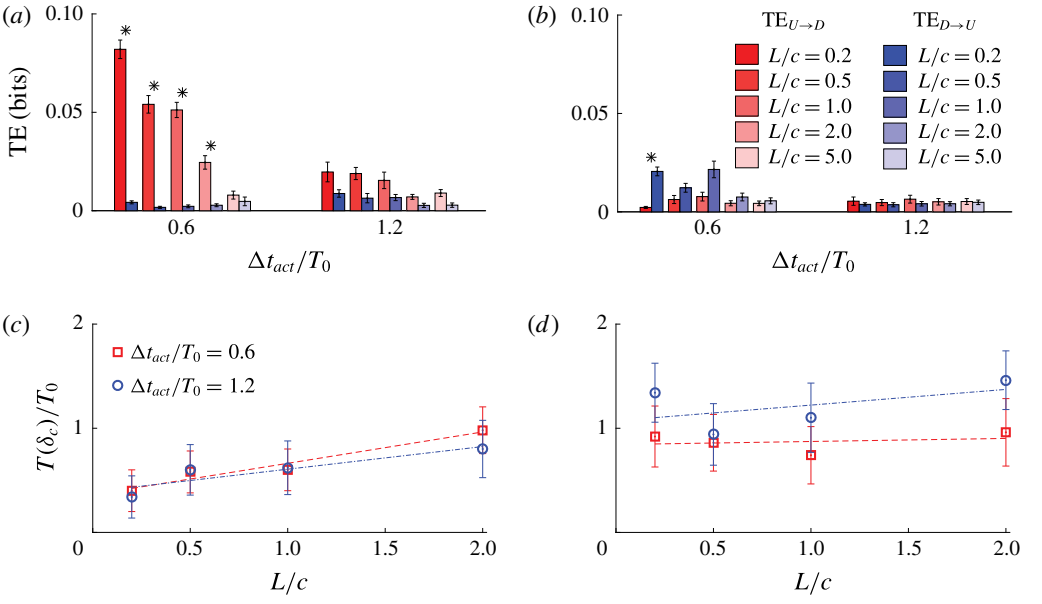


FIGURE 12. (Colour online) Effect of increasing the time interval between actuation events on transfer entropy and non-dimensional interaction delay for Upstream Active and Downstream Active: (*a*,*b*) $\mathrm{TE}_{U\to D}$ and $\mathrm{TE}_{D\to U}$, and (*c*,*d*) non-dimensional interaction time delay for Upstream Active (*a*,*c*) and Downstream Active (*b*,*d*) computed from time-series data of airfoils actuated with $\Delta t_{act}/T_0 = 0.6$ and 1.2, $m = 2$ and $f = 10$. Error bars represent standard errors. Asterisk in (*a*,*b*) identifies significant difference between $\mathrm{TE}_{U\to D}$ and $\mathrm{TE}_{D\to U}$ from paired *t*-tests (adjusted $p < 0.05$). For $\Delta t_{act}/T_0 = 0.6$ and $\Delta t_{act}/T_0 = 1.2$, we find that $\mathrm{TE}_{U\to D} > \mathrm{TE}_{D\to U}$ for Upstream Active for almost all combinations, and $\mathrm{TE}_{U\to D} < \mathrm{TE}_{D\to U}$ for Downstream Active for $\Delta t_{act}/T_0 = 0.6$, $L/c = 0.2$ and 1. Time delays in (*c*,*d*) are superimposed with linear regression fits, with colour coding shown in the legend.

stochastic processes, transfer entropy measures the extent to which predicting the future of one of the processes is enhanced from the knowledge of the other one. In this sense, this information-theoretic concept encapsulates salient dynamic information that could help in the quantification of a true causal link.

Toward a compelling demonstration of a transfer entropy approach to the study of fluid–structure interactions, we have focused on the archetypical problem of two tandem airfoils in a uniform flow. In a series of hypothesis-driven experiments, we have systematically varied the geometric configuration and actuation condition of the tandem airfoils, along with the computational set-up for evaluating transfer entropy. We demonstrated the possibility of predicting the directionality, extent and time scale of interactions from raw time series. Through an extensive robustness study, we determined the consistency of transfer entropy predictions with respect to the downsampling resolution of the time series, the number of symbols used for encoding the pitching dynamics of the airfoils, and the frequency of actuation of the airfoils.

In general, the idea of identifying causality from transfer entropy requires some caution (Lizier & Prokopenko 2010). 'Predictive information transfer', underlying Wiener's causality principle and inferred from transfer entropy, may differ from 'causal

https://doi.org/10.1017/jfm.2018.369 Published online by Cambridge University Press

information flow', which demands a direct manipulation of the experiment to assess whether a source variable will drive a destination variable. Through our controllable experimental framework, we demonstrate a profound relationship between predictive information transfer and causal information flow in hydrodynamic interactions between pitching airfoils. As the source and destination variables change in the experiment, our results reveal a concurrent, robust change in the landscape of transfer entropy.

Encouraged by these findings, future work aims at inferring causal structures underlying fish schooling. We will seek to quantify the extent of hydrodynamic interactions among fish in a school using time series of fish tail beat angles in transfer entropy analysis. We believe that the proposed model-free approach holds promise in revealing the role of hydrodynamics during the transition between a diamond and a phalanx school pattern.

In addition, we will aim to demonstrate the utility of transfer entropy for direct assessment of causality between a fluid flow and a solid structure. Transfer entropy computation using a direct measurement of a fluid feature, such as a velocity time trace, and motion of a structure may help assess the directionality and magnitude of the interaction. The introduction of transfer entropy in the study of fluid–structure interaction problems may benefit research in the broader context of fluid mechanics, such as the investigation of air flow–vocal folds interactions (Mittal, Erath & Plesniak 2013) and blade–vortex interactions (Rockwell 1998), where data-driven approaches have rarely been explored.

Acknowledgements

This work was supported by the National Science Foundation under grant numbers CBET-1332204 and CMMI-1433670 and by New York University Summer Research programme. The authors would like to thank A. Gementzopoulos for his help during the experiments and Dr S. Nakayama for useful feedback about the statistical design.

Supplementary materials

Supplementary materials are available at https://doi.org/10.1017/jfm.2018.369.

REFERENCES

ABDI, H. 2007 Bonferroni and Šidák corrections for multiple comparisons. In *Encyclopedia of Measurement and Statistics* (ed. N. Salkind), pp. 103–107. Sage.

ABDULSADDA, A. T. & TAN, X. 2012 An artificial lateral line system using IPMC sensor arrays. *Intl J. Smart Nano Mater.* **3** (3), 226–242.

ANDERSON, R. P., JIMENEZ, G., BAE, J. Y., SILVER, D., MACINKO, J. & PORFIRI, M. 2016 Understanding policy diffusion in the US: an information-theoretical approach to unveil connectivity structures in slowly evolving complex systems. *SIAM J. Appl. Dyn. Syst.* **15** (3), 1384–1409.

ASHRAF, I., BRADSHAW, H., HA, T.-T., HALLOY, J., GODOY-DIANA, R. & THIRIA, B. 2017 Simple phalanx pattern leads to energy saving in cohesive fish schooling. *Proc. Natl Acad. Sci. USA* **114** (36), 9599–9604.

BOSSOMAIER, T., BARNETT, L., HARR, M. & LIZIER, J. T. 2016 *An Introduction to Transfer Entropy: Information Flow in Complex Systems*. Springer.

BUTAIL, S., MWAFFO, V. & PORFIRI, M. 2016 Model-free information-theoretic approach to infer leadership in pairs of zebrafish. *Phys. Rev.* E **93** (4), 042411.

CONAWAY, M. R. 1989 Analysis of repeated categorical measurements with conditional likelihood methods. *J. Am. Stat. Assoc.* **84** (405), 53–62.

https://doi.org/10.1017/jfm.2018.369 Published online by Cambridge University Press

COVER, T. M. & THOMAS, J. A. 2006 *Elements of Information Theory*. Wiley.

DING, Y., NAWROTH, J. C., MCFALL-NGAI, M. J. & KANSO, E. 2014 Mixing and transport by ciliary carpets: a numerical study. *J. Fluid Mech.* **743**, 124–140.

DOWELL, E. H. & HALL, K. C. 2001 Modeling of fluid–structure interaction. *Annu. Rev. Fluid Mech.* **33** (1), 445–490.

FAES, L., PORTA, A., ROSSATO, G., ADAMI, A., TONON, D., CORICA, A. & NOLLO, G. 2013 Investigating the mechanisms of cardiovascular and cerebrovascular regulation in orthostatic syncope through an information decomposition strategy. *Autonomic Neurosci.: Basic Clinical* **178** (1), 76–82.

GRABOW, C., MACINKO, J., SILVER, D. & PORFIRI, M. 2016 Detecting causality in policy diffusion processes. *Chaos* **26** (8), 083113.

GRIFFITHS, S. W. & MAGURRAN, A. E. 1998 Sex and schooling behaviour in the Trinidadian guppy. *Animal Behav.* **56** (3), 689–693.

HLINKA, J., HARTMAN, D., VEJMELKA, M., RUNGE, J., MARWAN, N., KURTHS, J. & PALUŠ, M. 2013 Reliability of inference of directed climate networks using conditional mutual information. *Entropy* **15** (6), 2023–2045.

HOBECK, J. D. & INMAN, D. J. 2012 Artificial piezoelectric grass for energy harvesting from turbulence-induced vibration. *Smart Mater. Struct.* **21** (10), 105024.

HU, F., NIE, L.-J. & FU, S.-J. 2015 Information dynamics in the interaction between a prey and a predator fish. *Entropy* **17** (10), 7230–7241.

KIØRBOE, T., ANDERSEN, A., LANGLOIS, V. J. & JAKOBSEN, H. H. 2010 Unsteady motion: escape jumps in planktonic copepods, their kinematics and energetics. *J. R. Soc. Interface* **7** (52), 1591–1602.

KLEEMAN, R. 2002 Measuring dynamical prediction utility using relative entropy. *J. Atmos. Sci.* **59** (13), 2057–2072.

KLEEMAN, R. 2011 Information theory and dynamical system predictability. *Entropy* **13** (3), 612–649.

LAM, K., LI, J. Y. & SO, R. M. C. 2003 Force coefficients and Strouhal numbers of four cylinders in cross flow. *J. Fluids Struct.* **18** (3), 305–324.

LAMB, H. 1945 *Hydrodynamics*. Dover.

LIAO, J. C. 2007 A review of fish swimming mechanics and behaviour in altered flows. *Phil. Trans. R. Soc. Lond.* B **362** (1487), 1973–1993.

LIZIER, J. T. & PROKOPENKO, M. 2010 Differentiating information transfer and causal effect. *Eur. Phys. J.* B **73** (4), 605–615.

LÓPEZ, F., MATILLA-GARCÍA, M., MUR, J. & RUIZ-MARÍN, M. 2010 A non-parametric spatial independence test using symbolic entropy. *Regional Sci. Urban Economics* **40** (2), 106–115.

MAJDA, A., KLEEMAN, R. & CAI, D. 2002 A mathematical framework for quantifying predictability through relative entropy. *Meth. Appl. Anal.* **9** (3), 425–444.

MARSCHINSKI, R. & KANTZ, H. 2002 Analysing the information flow between financial time series. *Eur. Phys. J.* B **30** (2), 275–281.

MITTAL, R., ERATH, B. D. & PLESNIAK, M. W. 2013 Fluid dynamics of human phonation and speech. *Annu. Rev. Fluid Mech.* **45** (1), 437–467.

NAKAYAMA, S., RUIZ-MARÍN, M., CAMACHO, M. & PORFIRI, M. 2017 Plasticity in leader–follower roles in human teams. *Sci. Rep.* **7**, 14562.

ORANGE, N. & ABAID, N. 2015 A transfer entropy analysis of leader–follower interactions in flying bats. *Eur. Phys. J.* **224** (17–18), 3279–3293.

OZONO, S. 1999 Flow control of vortex shedding by a short splitter plate asymmetrically arranged downstream of a cylinder. *Phys. Fluids* **11** (10), 2928–2934.

PALUŠ, M. & VEJMELKA, M. 2007 Directionality of coupling from bivariate time series: how to avoid false causalities and missed connections. *Phys. Rev.* E **75** (5), 056211.

PARTRIDGE, B. L. 1982 The structure and function of fish schools. *Sci. Am.* **246** (6), 114–123.

PITCHER, T. J. 1998 Shoaling and shoaling behaviour in fishes. In *Comparative Psychology: A Handbook* (ed. G. Greenberg & M. M. Haraway), pp. 748–760. Garland.

PITCHER, T. J., MAGURRAN, A. E. & WINFIELD, I. J. 1982 Fish in larger shoals find food faster. *Behav. Ecol. Sociobiol.* **10** (2), 149–151.

https://doi.org/10.1017/jfm.2018.369 Published online by Cambridge University Press

PORFIRI, M. & RUIZ-MARÍN, M. 2017 Symbolic dynamics of animal interaction. *J. Theor. Biol.* **435**, 145–156.

PORFIRI, M. & RUIZ-MARÍN, M. 2018 Information flow in a model of policy diffusion: an analytical study. *IEEE Trans. Network Sci. Engng* **5** (1), 42–54.

POZRIKIDIS, C. 2010 Shear flow over cylindrical rods attached to a substrate. *J. Fluids Struct.* **26** (3), 393–405.

RISTROPH, L. & ZHANG, J. 2008 Anomalous hydrodynamic drafting of interacting flapping flags. *Phys. Rev. Lett.* **101** (19), 194502.

ROCKWELL, D. 1998 Vortex–body interactions. *Annu. Rev. Fluid Mech.* **30** (1), 199–229.

RUIZ-MARÍN, M., MATILLA-GARCÍA, M., CORDOBA, J. A. G., SUSILLO-GONZÁLEZ, J. L., ROMO-ASTORGA, A., GONZÁLEZ-PÉREZ, A., RUIZ, A. & GAYÁN, J. 2010 An entropy test for single-locus genetic association analysis. *BMC Genetics* **11** (1), 19.

SCHREIBER, T. 2000 Measuring information transfer. *Phys. Rev. Lett.* **85** (2), 461–464.

SHANNON, C. E. 1948 A mathematical theory of communication. *Bell Syst. Tech. J.* **27** (3), 379–423.

STANIEK, M. & LEHNERTZ, K. 2008 Symbolic transfer entropy. *Phys. Rev. Lett.* **100** (15), 158101.

STRYKOWSKI, P. J. & SREENIVASAN, K. R. 1990 On the formation and suppression of vortex shedding at low Reynolds numbers. *J. Fluid Mech.* **218**, 71–107.

TOMARU, T., MURAKAMI, H., NIIZATO, T., NISHIYAMA, Y., SONODA, K., MORIYAMA, T. & GUNJI, Y.-P. 2016 Information transfer in a swarm of soldier crabs. *Artif. Life Robot.* **21** (2), 177–180.

VICENTE, R., WIBRAL, M., LINDNER, M. & PIPA, G. 2011 Transfer entropy: a model-free measure of effective connectivity for the neurosciences. *J. Comput. Neurosci.* **30** (1), 45–67.

WEIHS, D. 1973 Hydromechanics of fish schooling. *Nature* **241** (5387), 290–291.

WIBRAL, M., PAMPU, N., PRIESEMANN, V., SIEBENHHNER, F., SEIWERT, H., LINDNER, M., LIZIER, J. T. & VICENTE, R. 2013 Measuring information-transfer delays. *PLoS One* **8** (2), e55809.

WIENER, N. 1956 The theory of prediction. *Mod. Math. Engrs* **1**, 125–139.

ZHANG, Z. & GRABCHAK, M. 2013 Bias adjustment for a nonparametric entropy estimator. *Entropy* **15** (6), 1999–2011.

https://doi.org/10.1017/jfm.2018.369 Published online by Cambridge University Press